Microporous and Mesoporous Materials 362 (2023) 112777

Contents lists available at ScienceDirect

Microporous and Mesoporous Materials

journal homepage: www.elsevier.com/locate/micromeso

# Thermal stability of templated ZSM-5 zeolites: An *in-situ* synchrotron X-ray powder diffraction study

Maura Mancinelli [a], Nicola Precisvalle [a], Matteo Ardit [a], Giada Beltrami [a], Lara Gigli [b], Enrico Catizzone [c,*], Massimo Migliori [c], Girolamo Giordano [c], Annalisa Martucci [a,**]

[a] Department of Physics and Earth Sciences, University of Ferrara Via Saragat 1, I-44121, Ferrara, Italy
[b] Elettra-Sincrotrone Trieste S.C.p.A., Beamline, Strada Statale 14 - Km 163, 5 in AREA Science Park, Basovizza, Trieste, Italy
[c] Chemical Engineering Catalysis and Sustainable Processes Laboratory, CECaSP_Lab - University of Calabria, Via P. Bucci, 87036, Rende, (CS), Italy

ARTICLE INFO

*Keywords:*
ZSM-5
$TPA^+$
*In situ* synchrotron X-ray powder diffraction
Thermal stability
Structural evolution

ABSTRACT

The topological symmetry of the as-synthesized ZSM-5 is orthorhombic *Pnma*, with 12 crystallographically independent tetrahedral sites in the unit cell. Highly crystallized ZSM-5 zeolite can be synthesized using organic species as structure directing agents (SDA), including tetra-*n*-propylammonium (TPA) and Na cations. This work investigates the thermal stability and high temperature structural evolution by *in situ* synchrotron (X-Ray) powder diffraction of TPA-ZSM-5 with different Si/Al ratios (15, 25, 50, and 100) and their structural modifications induced by template calcination. Rietveld refinements of the room temperature data revealed that in all samples tetrapropylammonium ions are located at the intersection of the sinusoidal and the straight channels. The refined $TPA^+$ content increases with the increasing of the Si/Al ratio of the zeolite, reaching the theoretical value of 4 when the Si/Al ratio = 84, in very good agreement with both chemical and thermogravimetric analyses. The bond distances evidenced the lack of interactions between the $TPA^+$ and the framework oxygen atoms. The high temperature refinements confirmed the high thermal stability of all four ZSM-5 samples, which remain crystalline until the end of the thermal treatment (800 °C). Burning of the template does not cause any relevant variations in the framework geometry and channel shape, confirming the high flexibility of the MFI framework.

In addition, thermal analysis proved insights about the effect of aluminum content on the interaction between SDA and zeolite structure.

## 1. Introduction

ZSM-5, the synthetic counterpart of the mutinaite mineral, $[Na_{2.76}K_{0.11}Mg_{0.21}Ca_{3.78}][Al_{11.20}Si_{84.91}]\cdot 60H_2O$ [1], is characterized by a MFI framework topology and a three-dimensional channels system. The structure is built on the intersection of two sets of tubular channels, both defined by 10-membered ring openings: the straight channel (SC channel), parallel to the [010] direction, and the sinusoidal channel (ZZ channel), parallel to the [100] direction. The free diameters of the SC and ZZ channels are from 5.4 to 5.6 Å and 5.1 to 5.5 Å, respectively [2]. The topological symmetry of the as-synthesized ZSM-5 (i.e., intended as ZSM-5 with tetrapropylammonium template molecule inside the channel system) is the orthorhombic *Pnma*, with 12 crystallographically independent tetrahedral sites in the unit cell [3], but its actual symmetry depends strongly on the synthesis and post-synthesis treatment, $SiO_2/Al_2O_3$ ratio, structural defects, temperature, nature and amount of sorbate organic molecules [4,5]. Usually, highly crystallized ZSM-5 zeolite can be synthesized using organic species as structure directing agents (SDA), including tetra-*n*-propylammonium (TPA) and Na cations. The type and amount of organic and inorganic precursors in synthetic solutions influence the Al location in the MFI zeolite framework and consequently the material properties. The use of TPA as SDA has attracted increasing attention due to its intermediate hydrophobicity/hydrophilicity and its ability to tailor the physicochemical properties (crystal size and/or chemical composition) of ZSM-5, thus optimizing the selectivity of zeolite catalysts and the efficiency of the overall chemical process [6]. In order to make the zeolite pores accessible to guest molecules, the organic templates have to be removed by

* Corresponding author.
** Corresponding author.
*E-mail addresses:* enrico.catizzone@unical.it (E. Catizzone), mrs@unife.it (A. Martucci).

https://doi.org/10.1016/j.micromeso.2023.112777
Received 22 June 2023; Received in revised form 4 August 2023; Accepted 18 August 2023
Available online 19 August 2023

**Table 1**
Si/Al ratio of templated ZSM-5 samples in gel and in bulk.

| Sample | Gel Si/Al ratio [mol/mol] | Bulk Si/Al ratio AAS [mol/mol] | Si/Al ratio EDX [mol/mol] |
|---|---|---|---|
| ZSM-5t_21 | 15 | 21 | 11 |
| ZSM-5t_30 | 25 | 30 | 13 |
| ZSM-5t_51 | 50 | 51 | 20 |
| ZSM-5t_84 | 100 | 84 | 43 |

**Table 2**
TPA $^{+}$ weight loss and theoretical calculation per unit cell.

| Sample | $Al^{3+}$ per u.c. [mol] | $TPA^{+}$ per u.c [mol] | $TPA^{+}$ under LT peak [% w/w] | $TPA^{+}$ under HT peak$^{-}$ [% w/w] | LT/(LT + HT) [−] |
|---|---|---|---|---|---|
| ZSM-5t_21 | 4.36 | 3.3 | 3.2% | 8.2% | 0.28 |
| ZSM-5t_30 | 3.10 | 3.5 | 3.7% | 7.6% | 0.33 |
| ZSM-5t_51 | 1.85 | 3.7 | 5.2% | 7.2% | 0.42 |
| ZSM-5t_84 | 1.13 | 4.0 | 6.0% | 7.0% | 0.46 |

calcination in air from 25 to 550 °C [7]. The template burning leaves behind one proton per each SDA complex for charge balancing, thus forming Brønsted acid sites. The comprehension of the template thermally induced decomposition at the molecular level is still a controversial issue and unambiguous interpretations have not yet been achieved. The targets of this work are to investigate the thermal stability and high temperature structural evolution of TPA-ZSM-5 with different Si/Al bulk ratios (21, 30, 51, and 84, respectively) and to study their structural modifications induced by template calcination on the zeolite framework by means of *in situ* synchrotron X-ray powder diffraction.

## 2. Materials and methods

**Materials.** ZSM-5 zeolite samples (MFI topology, 3-dimensional channels system) were synthesized at different Si/Al ratios starting from the following gel composition:

$$0.1Na_2O - 0.08TPABr - 1SiO_2 - x{\cdot}Al_2O_3 - 20H_2O$$

With the amount of $Al_2O_3$ varying in the range of $0.005 < x < 0.033$ mol, according to the expected Si/Al molar ratio in the gel, namely: 15, 25, 50 and 100 mol/mol. The synthesis gel was prepared by adding 2.66 g of sodium hydroxide (97%, Carlo Erba Reagenti) to 119.40 mL of distilled water [8–10]. Aluminum hydroxide (98%, Fluka) was dissolved in the basic solution with 7.10 g of tetrapropylammonium bromide (98%, Fluka), and the resulting solution was added to the gel. The addition of 19.95 g of precipitated silica (100%, Merck) was followed by stirring for 2 h at room temperature (*RT*). Crystallization was carried out at 175 °C in a PTFE-lined stainless steel static autoclave (0.150 L). After 96 h of crystallization, the solid phase was filtered, washed with distilled water and dried at 100 °C overnight. The bulk Si/Al molar ratio was determined by both atomic absorption spectroscopy using a GBC 932 instrument [11] and Energy-dispersive X-ray spectroscopy (Phenom ProX) and data are summarized in Table 1. TG/DTA data of as-synthesized samples were acquired (TA Instruments SDT 650) up to 850 °C (heating rate: 5 °C $min^{-1}$) under 100 mL/min of air flow. After calcination (air flow, 500 °C for 4 h), SEM-EDX of Na-form of the samples, were also acquired (Phenom Pro G6, Thermo Fisher) [12].

Even though the presence of extra-framework Al cannot be excluded (especially for samples with low Si/Al ratio), data shows an increasing of $TPA^{+}$ incorporation as counterion when increasing the Si/Al ratio of the zeolite, reaching the theoretical value of 4 when the Si/Al ratio is equal to 84.

**TDA-TGA analysis.** The charts are reported in Fig SI3 of Supplementary information and the TGA elaboration allows to calculate the TPA $^{+}$ weight loss for all the samples and the TPA $^{+}$ per unit cell, assuming the full incorporation of the Aluminum within the framework (Table 2).

A common feature of all the samples was found in a double peak in DTA analysis: a low-one (LT with the peak in the range: 414 °C–420 °C) related to the weak interaction of $TPA^{+}$ with a part of $AlO_4^{-}$ (and silanol groups) and a high-one (LT with the peak in the range: 471 °C–493 °C) attributed to the strong interaction with the rest of $AlO_4^{-}$. The deconvolution of the TGA derivative vs time allowed to attribute the relative amount of $TPA^{+}$ interacting with the zeolite structure in a weak and strong manner, respectively, and data reported in the last three columns of Table 2. Results indicate that fraction of weakly interacting $TPA^{+}$ increases as the aluminum content decreases. The higher fraction of strongly bonded $TPA^{+}$ can be associated to the TPA $^{+}$ interacting with $AlO_4^{-}$ framework species, according to the Al content increase in the samples.

SEM micrographs of the investigated samples are reported in Fig. SI4. All the samples exhibit prismatic larger crystals approximately 6–10 μm in size accompanied by smaller crystals approximately 1–2 μm.

**Synchrotron X-ray Powder Diffraction.** X-ray powder patterns as a function of temperature were collected at the MCX beamline [13,14] of the Elettra synchrotron light source (Trieste, Italy) in transmission geometry on a 4-circle Huber diffractometer equipped with a fast scintillator detector with a high-count rate, preceded by a pair of slits with a vertical aperture of 200 and 300 μm, respectively. Each sample was loaded into an axially spinning quartz capillary open at both ends (Ø = 0.5 mm) and previously mounted on a goniometric head. The sample temperature was varied and monitored using a gas blower (Oxford Danfysik DGB-0002). The experimental conditions for each temperature studied were λ = 0.82700(1) Å (15 keV), 2θ angular range = 3–45°, step size = 0.005° 2θ, counting time per step = 1 s. X-ray powder diffraction patterns were recorded every 100 °C from *RT* to 800 °C in air at a heating rate of 5 °C $min^{-1}$. The crystallinity change upon heating was obtained by the convolution through the Pawley's method by fitting the first peak at about 4.3° 2theta full 2θ range.

**Refinement Strategy.** Full-profile Rietveld refinements were performed using the GSAS software and the EXPGUI graphical interface [15,16]. The crystal structure of ZSM-5 collected at *RT* was refined starting from the structure model of the topological ZSM-5 (orthorhombic, s.g. *Pnma*) by Van Koningsveld et al. [3]. Peak profile modeling was performed using a pseudo-Voigt function with the peak cut-off set to 0.05% of the peak intensity maximum, two Gaussian terms (θ-independent *GW*, tan-θ dependent *GV*, respectively) and two Lorentzian broadening coefficients ($\cos\theta^{-1}$- and tanθ-dependent, *LX* and *LY*, respectively) plus an asymmetry contribution (*asym*) and two terms to reproduce the anisotropic contributions of the Lorentzian broadening (*ptec* and *stec*). In addition to 26 shifted Chebyshev polynomial coefficients to fit the background and a shift contribution (*shift*) to account for the sample displacement, the refinements included unit-cell parameters, atomic coordinates, and atomic displacement parameters (ADPs, $U_{iso}$). During the refinement of the framework atomic coordinates, a set of soft constraints were applied to the tetrahedral *T*–O and O–O bond distances (1.60 and 2.60 Å, respectively, with σ = 0.04 Å). The restraint weight (F) was progressively reduced in the final refinement cycles until the atomic coordinates were allowed to vary almost freely (*i.e.*, the calculated standard deviation of the bond lengths was smaller than the tolerance applied to the constrained bond distances). ADPs were constrained in order to have the same value for the same atomic species. The atomic coordinates of the tetrapropylammonium organic structure directing agent ($TPA^{+}$) were derived from residuals of the electron density calculated from the difference Fourier

**Table 3**
Details of XRPD data collection at *RT* and refinement agreement indices.

| $TPA^+$-ZSM-5 (s.g. *Pnma*, Z = 8) | | | | |
|---|---|---|---|---|
| $\lambda$ (Å) = 0.82700(1) | | | | |
| Refined $2\theta$ (°) range = 3–45 | | | | |
| No. of data = 8400 | | | | |
| No. of variable = 156 | | | | |
| | ZSM-5t_21 | ZSM-5t_30 | ZSM-5t_51 | ZSM-5t_84 |
| $R_{wp}$ | 0.216 | 0.156 | 0.140 | 0.188 |
| $R_p$ | 0.161 | 0.119 | 0.104 | 0.140 |
| $R_{F^2}$ | 0.102 | 0.128 | 0.124 | 0.102 |

maps. No residuals for H and Na atoms were detected due to both the low H atomic scattering factor and the high atomic disorder of H and Na within the zeolite lattice. The extra-framework atomic coordinates were refined by imposing soft constraints on the N–C (*i.e.,* 1.48 and 2.48 Å, σ = 0.04 Å) and C–C (*i.e.*, 1.42 and 2.70 Å, σ = 0.04 Å) bond distances to preserve the $TPA^+$ molecular geometry. In addition, the atomic fraction and ADPs for the N and C atoms of the $TPA^+$ molecule were constrained to vary equally.

Details of the data collection and refinement agreement factors are given in Table 3.

Framework atomic coordinates, site atomic fractions, and ADPs for samples at *RT* are reported as Supplemental Information (SI) in Tables SI1 to SI4. The atomic coordinates, site atomic fractions, and ADPs for the $TPA^+$ extra-framework molecule at *RT* are reported in Table SI5. In addition, Tables SI6 to SI21 list framework atomic coordinates, site atomic fractions, and ADPs for all investigated samples at selected temperatures (*i.e.*, 200, 400, 600, and 800 °C).

## 3. Results and discussion

**Structural Refinements at *RT*.** The crystal structure of ZSM-5 synthesized using $TPA^+$ molecules as templating agent, has been previously investigated by several authors [3,17–21]. All of these zeolites, as well as those investigated in this work, are characterized by the MFI structure, which crystallizes in the orthorhombic crystal system (s.g. *Pnma*) with 12 independent tetrahedral sites in the unit cell. A comparison between the investigated samples and those from the literature shows that the lattice parameters vary significantly with the aluminum content (*i.e.*, Si/Al ratio), with a volumetric variation ranging from 5332 $Å^3$ to 5379 $Å^3$ for samples with Si/Al ratios of 299 and 25 mol/mol, respectively (see Table 4). The tendency of a volumetric shrinkage as a function of Al content shown in Fig. 1 is expected from stoichiometric considerations. Indeed, the ionic radius of $Al^{3+}$ at the tetrahedral site is 50% larger than that of $Si^{4+}$ in the same coordination (i.e., 0.39 Å *vs.* 0.26 Å, respectively [22].

As far as the crystal structure at *RT* of the investigated ZSM-5 samples is concerned, subtle variations are observed with *T*–O bond distances and O–*T*–O bond angles ranging from 1.586(5) Å to 1.598(1) Å and from 108° to 110°, respectively (Tables SI22-SI25). On the contrary, the intertetrahedral *T*–O–*T* bond angles are characterized by a higher variability, suggesting that both the aluminum content and presence of $TPA^+$ molecules influence the geometry of the zeolite channels even at *RT*, exerting a kind of chemical pressure [23,24]. Indeed, the *T*–O–*T* bond angles range from 140 to 173°, with equivalent angles for the compared samples differing by less than 10° (Tables SI22-SI25).

The channel distortions in zeolite systems are usually quantified as the departure from an ideal channel with a circular cross section, i.e., by calculating the ellipticity parameter $\varepsilon$, which is defined as the ratio between the longest and the shortest O–O bond distances that define the minimum and the maximum channel diameters, respectively. The data shown in Table 5 indicate that the straight (SC) and sinusoidal entrance (ZZ-A) channels are quite distorted ($\varepsilon$ = 1.09 on average), while the sinusoidal exit (ZZ-B) is more regular ($\varepsilon$ = 1.04 on average). These distortions are strongly related to the location of $TPA^+$ molecules, showing the propyl-N-propyl fragments pointing into the sinusoidal and straight channels both in a non-extended conformation. These values, as well as other structural parameters, seem to be little or unaffected by the aluminum content. The crystallographic free area (CFA) sensu Baerlocher (*i.e.*, calculates as $\pi \times$ (channel mean radius)$^2$ in $Å^2$ [25], shows that the channel type have a different CFA. On average, CFA(ZZ-A) = 22.9 $Å^2$, CFA(SC) = 23.6 $Å^2$, CFA(ZZ-B) = 24.1 $Å^2$, with sinusoidal channels characterized by the smallest (ZZ-A) and the largest (ZZ-B)

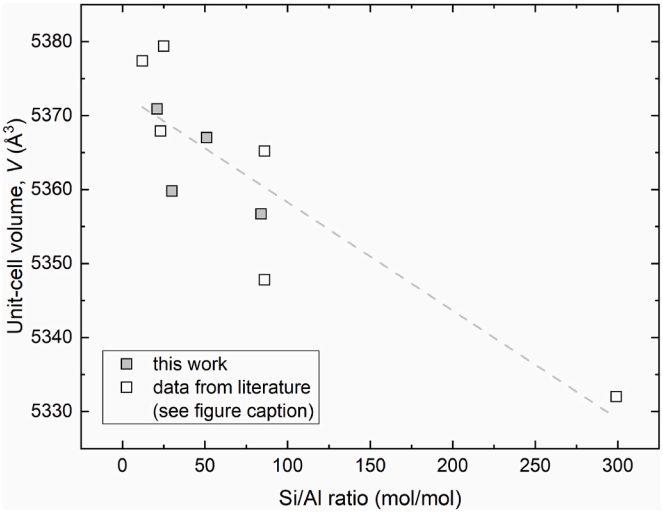


**Fig. 1.** Unit cell volume as a function of Si/Al ratio. Unit-cell volume and Si/Al ratio refer to data reported in Table 3. Dashed lines are a reader's guide. Symbol sizes exceed the estimated measurements uncertainties.

**Table 5**
Ellipticity ($\varepsilon$) and crystallographic free area (CFA) parameters for the investigated zeolite samples at *RT*.

| | Channel | ZSM-5t_21 | ZSM-5t_30 | ZSM-5t_51 | ZSM-5t_84 |
|---|---|---|---|---|---|
| $\varepsilon$ | SC | 1.082 | 1.104 | 1.084 | 1.080 |
| | ZZ-A | 1.086 | 1.085 | 1.078 | 1.083 |
| | ZZ-B | 1.037 | 1.045 | 1.050 | 1.040 |
| CFA ($Å^2$) | SC | 23.56 | 23.61 | 23.65 | 23.60 |
| | ZZ-A | 22.95 | 22.90 | 22.84 | 22.79 |
| | ZZ-B | 24.30 | 24.22 | 24.03 | 24.02 |

**Table 4**
Unit-cell parameters of ZSM-5 zeolites at *RT* synthesized via *n*$TPA^+$ templating molecule (0 < *n* < 4 molecules per unit cell pore-fillings).

| $TPA^+$-ZSM-5 (s.g. *Pnma*, Z = 8) | | | | | | | | | | |
|---|---|---|---|---|---|---|---|---|---|---|
| | ZSM-5t_21 | ZSM-5t_30 | ZSM-5t_51 | ZSM-5t_84 | Ref. [17] | Ref. [15] | Ref. [16] | Ref. [14] | Ref. [18] | Ref. [3] |
| *a* (Å) | 20.048(4) | 20.044(4) | 20.062(3) | 20.049(1) | 20.092 | 20.072 | 20.100 | 20.07 | 20.044 | 20.022 |
| *b* (Å) | 19.966(4) | 19.939(4) | 19.945(3) | 19.933(1) | 19.952 | 19.937 | 19.959 | 19.92 | 19.918 | 19.899 |
| *c* (Å) | 13.418(2) | 13.411(3) | 13.413(2) | 13.404(1) | 13.414 | 13.414 | 13.409 | 13.42 | 13.395 | 13.383 |
| *V* ($Å^3$) | 5370.9(2) | 5359.8(2) | 5367.0(4) | 5356.7(7) | 5377.4 | 5367.9 | 5379.4 | 5365.2 | 5347.8 | 5332.0 |
| Si/Al | 21 | 30 | 51 | 84 | 12 | 23 | 25 | 86 | 86 | 299 |

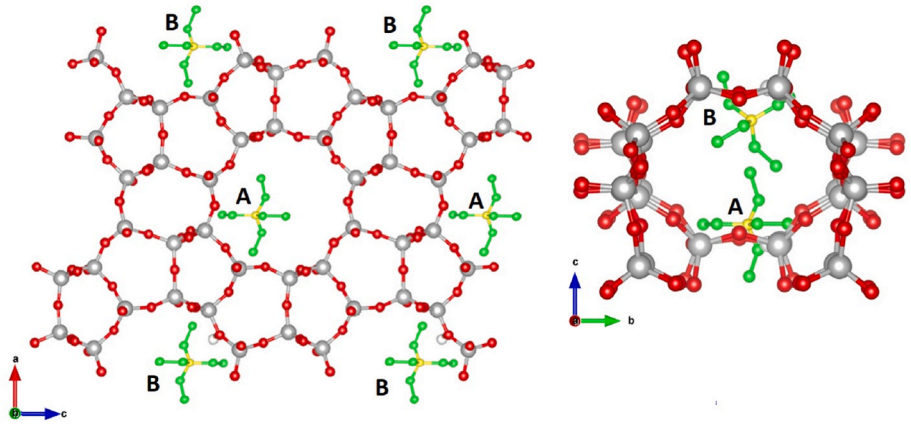


**Fig. 2.** Polyhedral representation of the ZSM-5 structure along the [010] and [100] direction, respectively. $TPA^+$ is located at the intersection of the straight and sinusoidal channels. A and B refer to the possible orientations of $TPA^+$.

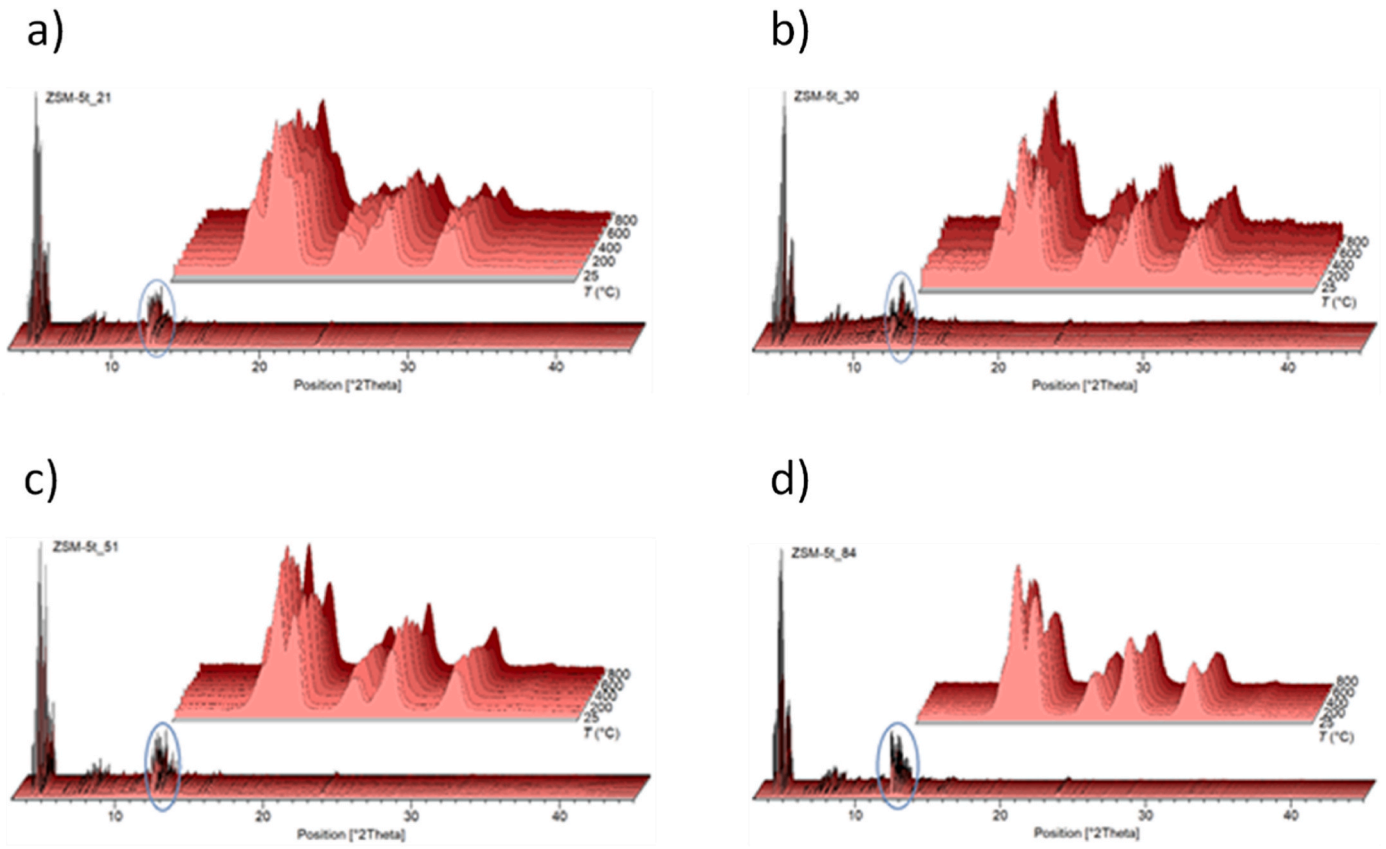


**Fig. 3.** Cascade plots of ZSM-5t_21, ZSM-5t_30, ZSM-5t_51, and ZSM-5t_84 zeolites (from *a* to *d*, respectively), and pattern details in the 4–5° and 10–15° 2θ angular ranges, within insets.

CFA, respectively.

According to Van Koningsveld et al. [3], residuals of electron density calculated using difference Fourier maps suggest that the $TPA^+$ molecule is located at the intersection of the sinusoidal and straight channels. Due to the presence of a mirror plane *m* at the center of the $TPA^+$ molecule, the molecule can statistically adopt two different crystallographic orientations depending on the distribution of the four propyl groups around the central nitrogen (Fig. 2).

Rietveld refinements of the atomic occupancy indicate that the as-synthesized ZSM-5 sample with the Si/Al ratio equal to 84 contains four molecules per unit cell of $TPA^+$ molecules, *i.e.*, the maximum theoretical number of $TPA^+$ molecules within the channels for a ZSM-5 zeolite [26].

In the other samples, the refined $TPA^+$ content decreases with the lowering of the Si/Al ratio of the zeolite (~3.3, 3.5 and 3.7 molecules per unit cell in ZSM-5 samples with Si/Al equals to 21, 30 and 51, respectively), –in very good agreement with both chemical (Table 1) and thermogravimetric analyses (Table 2). Since no additional electron density residuals were detected from the Fourier map calculation, it can be argued that no co-adsorbed water molecules are present within the zeolite lattice.

**High Temperature (*HT*) Structural Refinements.** Information on the kinetics of $TPA^+$ decomposition, as well as structural variations due to the release of extra-framework components and the resulting

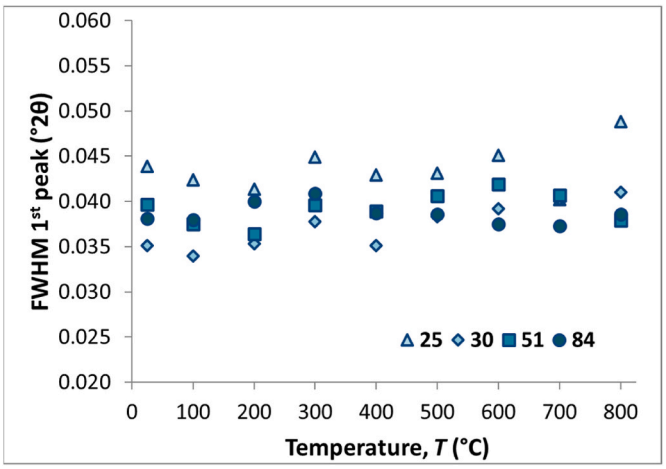


**Fig. 4.** Evolution of the full width at half maximum (FWHM) of XRD peak at ~4.3° 2theta for all the investigated samples.

framework rearrangement, can be determined from *in-situ* X-ray diffraction data collected at *HT*. The cascade plots in Fig. 3 show the evolution of the investigated as-synthesized ZSM-5 samples in the temperature range *RT*–800 °C.

No evidence of crystallinity loss (peak broadening or collapse) is observed up to 800 °C, demonstrating the high thermal stability of all as-synthesized ZSM-5 samples (Fig. 4).

Temperature-induced variations in both peak positions and intensities are observed for all samples investigated. In particular, up to about 300 °C, peaks shift to lower 2θ angles, while at higher temperatures a peak shift to higher 2θ angles is observed. This means that an initial lattice expansion (up to 300 °C) is followed by a unit-cell reduction up to the maximum investigated temperature. A lattice contraction can be related to the progressive removal of organic molecules during a thermal decomposition process [27–30]. Further clues to this process can be derived from the peak intensity variations (mainly related to changes in structural parameters) upon heating, as will be discussed later. The variation of the lattice parameters and the unit-cell volume as a function of temperature (normalized to their value at *RT*) is shown in Fig. 5.

Based on their thermal evolution and according to the aluminum content, two different trends can be rationalized for the pair of samples ZSM-5t_21 - ZSM-5t_30, and ZSM-5t_51 - ZSM-5t_84. In agreement with Sen et al. [31], the concentration of $Al^{3+}$ ions seems to be a discriminating factor during the thermal evolution of orthorhombic H-ZSM-5 zeolites. Although at different rates, all investigated zeolite samples are initially affected (to a lesser extent for the sample ZSM-5t_84) by a temperature-induced positive thermal expansion up to 200 °C. At higher temperatures, the pairs of samples ZSM-5t_21 - ZSM-5t_30, and ZSM-5t_51 - ZSM-5t_84 behave differently, with samples ZSM-5t_21 and ZSM-5t_30 (those characterized by the highest aluminum content) undergoing a regular volumetric contraction up to 800 °C. Differently, samples ZSM-5t_51 and ZSM-5t_84 show a steep volumetric drop up to 300 °C, followed by a more gradual volumetric contraction up to 700 °C. In agreement with Sen et al. [31], all samples show a negative thermal expansion in the 200–700 °C temperature range. At the highest temperatures studied (*i.e.*, from 700 to 800 °C), samples ZSM-5t_51 and ZSM-5t_84 are characterized by a volumetric expansion. The total volume reduction over the investigated thermal range is 0.87% and 0.89% for samples ZSM-5t_21 and ZSM-5t_30, and 0.75% and 0.71% for samples ZSM-5t_51 and ZSM-5t_84, i.e., the lower the $Al^{3+}$ content, the lower the cell volume reduction. This trend is consistent with that observed for a high-silica orthorhombic polymorph of H-ZSM-5 (Si/Al = 140) and for a silicalite-1 sample [32,33], where a volume reduction of 0.52% was found in the same temperature range. Fig. 6 shows the

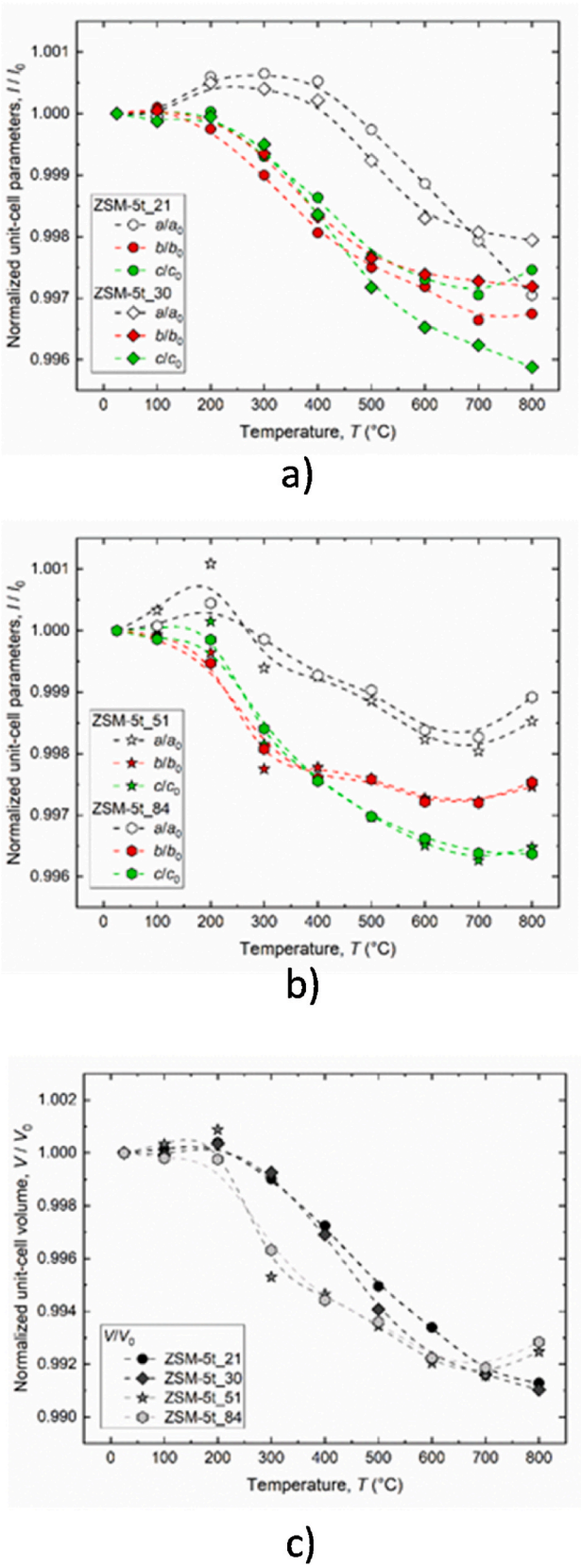


**Fig. 5.** Lattice parameters evolution with temperature for samples ZSM-5t_21, and ZSM-5t_30 (*a*) and ZSM-5t_51 and ZSM-5t_84 (*b*), and temperature-dependence of unit-cell volume for all as-synthetized ZSM-5 samples (*c*).

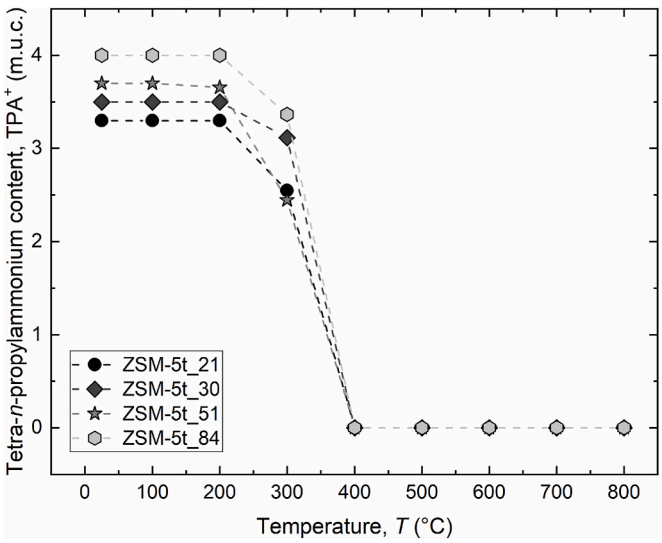


**Fig. 6.** Content of extra-framework $TPA^+$ molecules as a function of temperature.

variation of the $TPA^+$ content as a function of temperature.

Refinement of the site atomic fractions (site occupancies) shows that the crystallographic sites hosting the templating molecule are unchanged up to 200 °C. At higher temperatures, the decomposition and release process of $TPA^+$ takes place for all the samples studied and, although with some small differences, it is completed at 400 °C when all the crystallographic sites are completely empty. The degradation of the $TPA^+$ between 200 °C and 400 °C could explain the enhanced volumetric reduction observed for the samples in this temperature range. When the $TPA^+$ degradation and expulsion of the decomposition product are complete, the framework can relaxes due to the disappearing of the inward negative pressure. This mechanism explains the evolution of the unit cell parameters and the positive cell volume expansion from 700 °C to 800 °C.

.The three-dimensional arrangement of tetrahedra sharing corners in ZSM-5 zeolite structures confers a high framework flexibility. In fact, all the investigated samples, although subjected to a high thermal regime, show slight variations in both *T*–O bond distances and *T*–O–*T* bond angles, indicating that their framework does not undergo relevant structural distortions.

The *T*–O bond distances and *T*–O–*T* bond angles for selected temperatures (*i.e.*, 200, 400, 600, and 800 °C) are listed in Tables SI22-SI25. This is also evidenced by the temperature variation of the ellipticity parameter for zeolite channels. While the ellipticity of ZZ-B channels is almost constant for all the samples over the whole temperature range (*i.e.*, $\varepsilon$ around 1.4), the heating process induces a variation in the shape of both ZZ-A and SC channels (Fig. 7). In particular, two opposite trends can be observed: an increase in the ellipticity of the ZZ-A channel (evidence of a progressive departure from the circular shape) is associated with a decrease in the ellipticity (regularization) of the SC channel. Although some inhomogeneous variations can be observed for samples ZSM-5t_21 and ZSM-5t_51 due to the depletion of $TPA^+$ at the earlier heating stages (*i.e.*, between 200 and 300 °C), the 10 MR channel of all

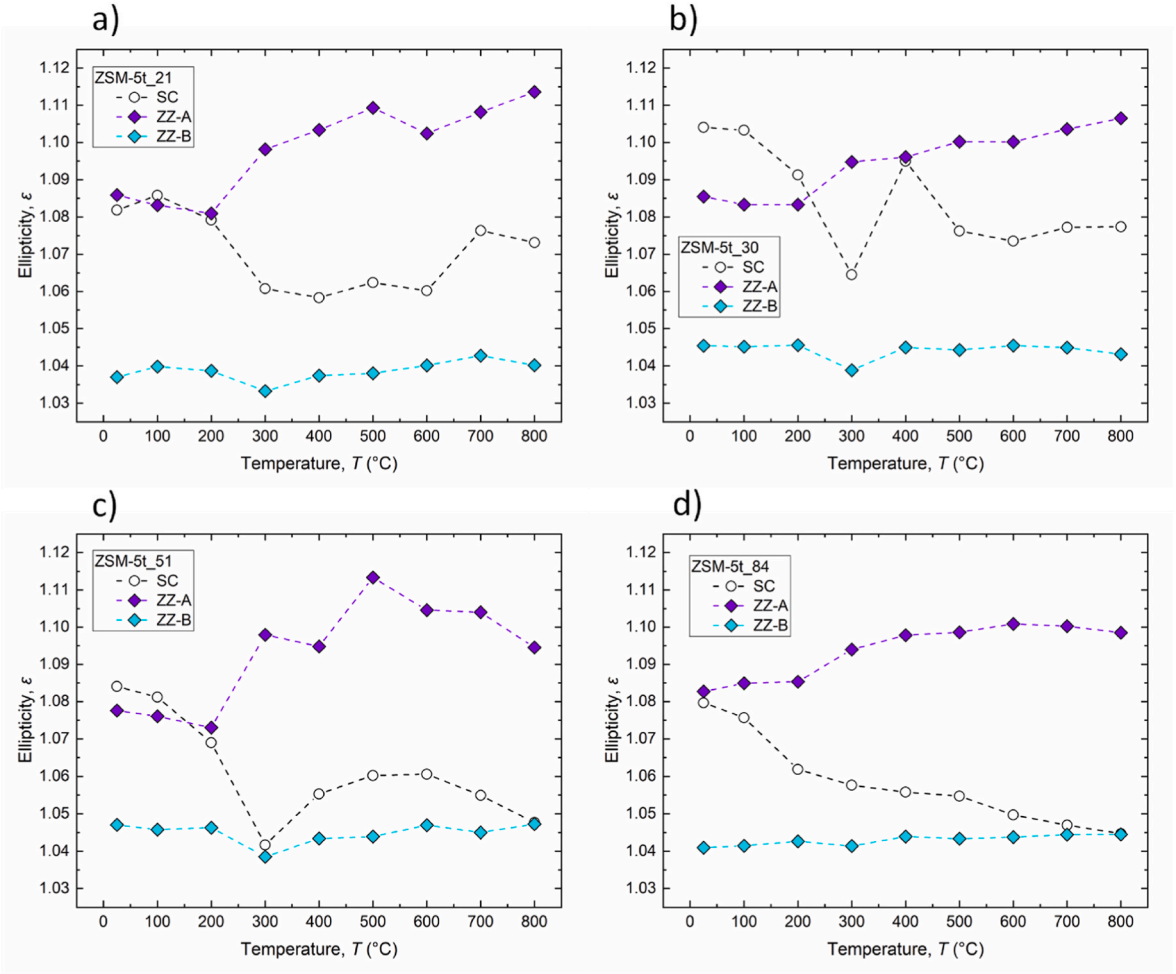


**Fig. 7.** Ellipticity evolution of samples ZSM-5t_21 (a), ZSM-5t_30 (b), ZSM-5t_51 (c) and ZSM-5t_84 (d) at *HT*.

the samples studied tends to become more regular, although never reaching a circular shape. This transient regularization can be reasonably attributed to the pressure of the volatile products produced by the degradation of the template formed inside. They must diffuse along 10 MR channel, and their slow diffusion develops a significant internal pressure thus causing the corresponding transient expansion of the 10 MR channel.

The thermal treatment also induced slight changes in the CFA of the as-synthetized ZSM-5 zeolites (Fig. SI2). Evidence of pore diameter reduction upon heating can be inferred from the decrease in CFA values for both SC and ZZ-A channels. In contrast, the effect of the heating process is less pronounced in the ZZ-B channel.

## 4. Conclusions

*In situ* synchrotron powder diffraction allowed monitoring the progressive thermal activation of four $TPA^+$ templated ZSM-5 characterized by different Si/Al ratios. Rietveld refinements of the room temperature data highlighted that in all the samples tetrapropylammonium ions are located at the intersection of the sinusoidal and the straight channels. The refined $TPA^+$ content increases with the increasing of the zeolite Si/Al ratio, reaching the theoretical value of 4 when the Si/Al ratio = 84, –in very good agreement with both chemical and thermogravimetric analyses. The analysis of the bond distances evidenced the lack of interactions between the $TPA^+$ and the framework oxygen atoms. Furthermore, the ellipticity parameters showed that the geometry of the channels is slightly distorted since the beginning of the thermal treatment. The high temperature refinements confirmed the high thermal stability of all four ZSM-5 samples, which remain crystalline until the end of the thermal treatment (800 °C). The complete activation of ZSM-5 occurs between 300 and 400 °C, when the $TPA^+$ template is completely removed from the pores. Burning of the template does not cause any relevant variations in the framework geometry and channel shape, confirming the high flexibility of the MFI framework.

## CRediT authorship contribution statement

**Maura Mancinelli:** Writing – original draft, Investigation, Data curation. **Nicola Precisvalle:** Investigation, Formal analysis. **Matteo Ardit:** Software, Data curation. **Giada Beltrami:** Validation, Conceptualization. **Lara Gigli:** Methodology, Investigation. **Enrico Catizzone:** Writing – review & editing, Data curation. **Massimo Migliori:** Writing – review & editing, Conceptualization. **Girolamo Giordano:** Resources, Conceptualization. **Annalisa Martucci:** Writing – review & editing, Supervision, Project administration.

## Declaration of competing interest

The authors declare that they have no known competing financial interests or personal relationships that could have appeared to influence the work reported in this paper.

## Data availability

Data will be made available on request.

## Acknowledgments

Project funded under the National Recovery and Resilience Plan (NRRP), Mission 04 Component 2 Investment 1.5 – NextGenerationEU, Call for tender n. 3277 dated 30/12/2021, Award Number: 0001052 dated 23/06/2022.

## Appendix A. Supplementary data

Supplementary data to this article can be found online at https://doi.org/10.1016/j.micromeso.2023.112777.

## References

[1] G. Vezzalini, S. Quartieri, E. Galli, A. Alberti, G. Cruciani, Å. Kvick, Crystal structure of the zeolite mutinaite, the natural analog of ZSM-5, Zeolites 19 (1997) 323–325, https://doi.org/10.1016/S0144-2449(97)00124-3.
[2] H. Van Koningsveld, J.C. Jansen, A.J.M. De Man, Single-crystal Structure Analysis and Energy Minimizations of a MFI-type Zeolite at Low P-Dichlorobenzene Sorbate Loading, 52, 1996, pp. 131–139, https://doi.org/10.1107/S0108768195008512. Urn:Issn:0108-7681.
[3] H. Van Koningsveld, H. Van Bekkum, J.C. Jansen, On the Location and Disorder of the Tetrapropylammonium (TPA) Ion in Zeolite ZSM-5 with Improved Framework Accuracy, 43, Urn, 1987, pp. 127–132, https://doi.org/10.1107/S0108768187098173. :Issn:0108-7681.
[4] H. van Koningsveld, F. Tuinstra, J.C. Jansen, H. van Bekkum, On the preparation of a monoclinic (nearly) single crystal of zeolite HZSM-5, Zeolites 9 (1989) 253–256, https://doi.org/10.1016/0144-2449(89)90035-3.
[5] H. van Koningsveld, J.C. Jansen, H. van Bekkum, The monoclinic framework structure of zeolite H-ZSM-5. Comparison with the orthorhombic framework of as-synthesized ZSM-5, Zeolites 10 (1990) 235–242, https://doi.org/10.1016/0144-2449(94)90134-1.
[6] M. Moliner, F. Rey, A. Corma, Towards the rational design of efficient organic structure-directing agents for zeolite synthesis, Angew. Chem. Int. Ed. 52 (2013) 13880–13889, https://doi.org/10.1002/ANIE.201304713.
[7] I. Jirka, P. Sazama, A. Zikánová, P. Hrabánek, M. Kocirik, Low-temperature thermal removal of template from high silica ZSM-5. Catalytic effect of zeolitic framework, Microporous Mesoporous Mater. 137 (2011) 8–17, https://doi.org/10.1016/J.MICROMESO.2010.08.015.
[8] M. Migliori, A. Aloise, E. Catizzone, G. Giordano, Kinetic analysis of methanol to dimethyl ether reaction over H-MFI catalyst, Ind. Eng. Chem. Res. 53 (2014) 14885–14891, https://doi.org/10.1021/IE502775U/SUPPL_FILE/IE502775U_SI_001.PDF.
[9] A. Aloise, A. Marino, F. Dalena, G. Giorgianni, M. Migliori, L. Frusteri, C. Cannilla, G. Bonura, F. Frusteri, G. Giordano, Desilicated ZSM-5 zeolite: catalytic performances assessment in methanol to DME dehydration, Microporous Mesoporous Mater. 302 (2020), 110198, https://doi.org/10.1016/J.MICROMESO.2020.110198.
[10] G. Bonura, C. Cannilla, L. Frusteri, E. Catizzone, S. Todaro, M. Migliori, G. Giordano, F. Frusteri, Interaction effects between CuO-ZnO-ZrO2 methanol phase and zeolite surface affecting stability of hybrid systems during one-step CO2 hydrogenation to DME, Catal. Today 345 (2020) 175–182, https://doi.org/10.1016/J.CATTOD.2019.08.014.
[11] E. Catizzone, A. Aloise, M. Migliori, G. Giordano, Dimethyl ether synthesis via methanol dehydration: effect of zeolite structure, Appl. Catal. Gen. 502 (2015) 215–220, https://doi.org/10.1016/J.APCATA.2015.06.017.
[12] P. Lanzafame, G. Papanikolaou, S. Perathoner, G. Centi, M. Migliori, E. Catizzone, A. Aloise, G. Giordano, Direct versus acetalization routes in the reaction network of catalytic HMF etherification, Catal. Sci. Technol. 8 (2018) 1304–1313, https://doi.org/10.1039/C7CY02339A.
[13] J.R. Plaisier, L. Nodari, L. Gigli, E.P.R.S. Miguel, R. Bertoncello, A. Lausi, The X-ray diffraction beamline MCX at Elettra: a case study of non-destructive analysis on stained glass, Acta IMEKO 6 (2017) 71–75, https://doi.org/10.21014/ACTA_IMEKO.V6I3.464.
[14] L. Rebuffi, J.R. Plaisier, M. Abdellatief, A. Lausi, A.P. Scardi, MCX: a synchrotron radiation beamline for X-ray diffraction line profile analysis, Z. Anorg. Allg. Chem. 640 (2014) 3100–3106, https://doi.org/10.1002/ZAAC.201400163.
[15] A.C. Larson, R.B. Von, D. Lansce, GSAS GENERAL STRUCTURE ANALYSIS SYSTEM, ((n.d.)).
[16] B.H. Toby, IUCr, EXPGUI, a Graphical User Interface for GSAS, 34, 2001, pp. 210–213, https://doi.org/10.1107/S0021889801002242. Urn:Issn:0021-8898.
[17] D.H. Olson, G.T. Kokotailo, S.L. Lawton, W.M. Meier, Crystal structure and structure-related properties of ZSM-5, J. Phys. Chem. 85 (1981) 2238–2243, https://doi.org/10.1021/J150615A020/SUPPL_FILE/J150615A020_SI_001.PDF.
[18] Y. Yokomori, S. Idaka, The structure of TPA-ZSM-5 with Si/Al=23, Microporous Mesoporous Mater. 28 (1999) 405–413, https://doi.org/10.1016/S1387-1811(98)00311-4.
[19] K.J. Chao, J.C. Lin, Y. Wang, G.H. Lee, Single crystal structure refinement of TPA ZSM-5 zeolite, Zeolites 6 (1986) 35–38, https://doi.org/10.1016/0144-2449(86)90009-6.
[20] H. Lermer, M. Draeger, J. Steffen, K.K. Unger, Synthesis and structure refinement of ZSM—5 single crystals, Zeolites 5 (1985) 131–134, https://doi.org/10.1016/0144-2449(85)90019-3.
[21] G.D. Price, J.J. Pluth, J.V. Smith, J.M. Bennett, R.L. Patton, Crystal structure of tetrapropylammonium fluoride containing precursor to fluoride silicalite, J. Am. Chem. Soc. 104 (1982) 5971–5977, https://doi.org/10.1021/JA00386A023/SUPPL_FILE/JA00386A023_SI_001.PDF.
[22] R.D. Shannon, IUCr, Revised Effective Ionic Radii and Systematic Studies of Interatomic Distances in Halides and Chalcogenides, 32, Urn, 1976, pp. 751–767, https://doi.org/10.1107/S0567739476001551. Issn:0567-7394.
[23] A. Lobato, H.H. Osman, M.A. Salvadó, M. Taravillo, V.G. Baonza, J.M. Recio, Chemical pressure–chemical knowledge: squeezing bonds and lone pairs within the valence shell electron pair repulsion model, Phys. Chem. Chem. Phys. 21 (2019) 12585–12596, https://doi.org/10.1039/C9CP00913B.

[24] H.H. Osman, M.A. Salvadó, P. Pertierra, J. Engelkemier, D.C. Fredrickson, J. M. Recio, Chemical pressure maps of molecules and materials: merging the visual and physical in bonding analysis, J. Chem. Theor. Comput. 14 (2018) 104–114, https://doi.org/10.1021/ACS.JCTC.7B00943/ASSET/IMAGES/LARGE/CT-2017-00943E_0011 (JPEG).
[25] L.B. McCusker, D.H. Olson, C. Baerlocher, Atlas of Zeolite Framework Types, Atlas of Zeolite Framework Types, 2007, https://doi.org/10.1016/B978-0-444-53064-6.X5186-X.
[26] P. Fejes, J.B. Nagy, J. Halász, A. Oszkó, Heat-treatment of isomorphously substituted ZSM-5 zeolites and its structural consequences: an X-ray diffraction, 29Si MAS-NMR, XPS and FT-IR spectroscopy study, Appl. Catal. Gen. 175 (1998) 89–104, https://doi.org/10.1016/S0926-860X(98)00212-9.
[27] G. Cruciani, Zeolites upon heating: factors governing their thermal stability and structural changes, J. Phys. Chem. Solid. 67 (2006) 1973–1994, https://doi.org/10.1016/J.JPCS.2006.05.057.
[28] M. Milanesio, G. Artioli, A.F. Gualtieri, L. Palin, C. Lamberti, Template Burning inside TS-1 and Fe-MFI Molecular Sieves: an in Situ XRPD Study, 2003, https://doi.org/10.1021/JA037229.
[29] L. Leardini, A. Martucci, A. Alberti, G. Cruciani, Template burning effects on stability and boron coordination in boron levyne studied by in situ time resolved synchrotron powder diffraction, Microporous Mesoporous Mater. 167 (2013) 117–126, https://doi.org/10.1016/J.MICROMESO.2012.02.013.
[30] A. Martucci, M. de L. Guzman-Castillo, F. Di Renzo, F. Fajula, A. Alberti, Reversible channel deformation of zeolite omega during template degradation highlighted by in situ time-resolved synchrotron powder diffraction, Microporous Mesoporous Mater. 104 (2007) 257–268, https://doi.org/10.1016/J.MICROMESO.2007.02.040.
[31] S. Sen, R.R. Wusirika, R.E. Youngman, High temperature thermal expansion behavior of H[Al]ZSM-5 zeolites: the role of Brønsted sites, Microporous Mesoporous Mater. 87 (2006) 217–223, https://doi.org/10.1016/J.MICROMESO.2005.08.010.
[32] M. Ardit, A. Martucci, G. Cruciani, Monoclinic orthorhombic phase transition in ZSM 5 zeolite: spontaneous strain variation and thermodynamic properties, J. Phys. Chem. C 119 (2015) 7351–7359, https://doi.org/10.1021/ACS.JPCC.5B00900/ASSET/IMAGES/JP-2015-00900A_M015 (GIF).
[33] D.S. Bhange, V. Ramaswamy, Negative thermal expansion in silicalite-1 and zirconium silicalite-1 having MFI structure, Mater. Res. Bull. 41 (2006) 1392–1402, https://doi.org/10.1016/J.MATERRESBULL.2005.12.002.